ADVANCED MATERIALS

DOI: 10.1002/adma.200701021

Superelastic and Spring Properties of Si_3N_4 Microcoils**

By *Chuanbao Cao,* Hongli Du, Yajie Xu, Hesun Zhu, Taihua Zhang,* and *Rong Yang*

Ceramics have many excellent characteristics, such as high refractoriness, hardness, compressive strength and chemical stability. It is well known that brittleness is a definitive defect of ceramic materials and this is the greatest drawback in making ceramics available as engineering materials. Great efforts have been made on the increase of ceramics toughness to overcome this defect for the sake of extending the application range of ceramics. As an elastic device, the highest toughness representative, springs have attracted extensive attention.[1] Producing a ceramic with spring properties is a dream for ceramic researchers.

As an important member of ceramics, silicon nitride (Si_3N_4) is characterized by its direct band gap of 5.3 eV and has been proved to be the active components for device applications due to its high strength, lightweight, and good resistance against thermal shock and oxidation.[2,3] Various morphologies of Si_3N_4 in the nano- or micrometer scale[4–9] have been explored in the last few years because of their potentials in applications where mechanical strength and high temperature/corrosive durability are required. Compared with other configurations, such as wires, tubes and belts, helical springs observed in a number of inorganic materials[10–20] are expected to have remarkable properties in some aspects. For example, helical spring structures having dimensions on the order of nano- or micrometers are expected to have remarkable mechanical properties due to their helicity and periodicity or as a novel reinforcement in high strain composites. The ability to produce springs from ceramic components opens up new routes for ceramics which allow the production of microdevice for MEMS, motors, electromagnets generators and related equipment. Coiled Si_3N_4 fibers have been prepared from a gas mixture by S. Motojima et al.[21–23] and the dimensions of them were 2 to 5 μm in coil pitch (H), 10 to 15 μm in coil diameter (D) and 50–100 μm in coil length (L). They once attempted to clarify the spring characteristics of the coiled fibers. But they only observed that the microcoil fractured when stretched to a certain degree and the essential parameters of spring were not represented. In other inorganic materials research, although super-lattice structured ZnO nanohelics have been synthesized and can be pulled to an almost straightened shape, however, the repeating loading effect on the shape recovery haven't been performed.[24] So, although they obtained nano- or microcoils of inorganic materials, whether the inorganic materials or ceramics nano- or microcoils had springs properties could not be confirmed. There is still questionable whether the ceramic coils can endure repeating loadings without causing permanent distortion. Current work in this paper is to confirm the normal spring mechanical properties of Si_3N_4 microcoils based on large-scale preparation by a comparatively safe and cheap route. Moreover, different from traditional steel springs, the Si_3N_4 microcoils also well demonstrate their superelasticity.

We firstly prepared large scale of Si_3N_4 microcoils by CVD method. The synthesized Si_3N_4 microcoils had the dimensions of $d = 0.5$–4 μm, $D = 8$–300 μm, $H = 6$–500 μm, and the coil length of the microcoil could reach as long as several millimeters. The XRD pattern of the as-synthesized products indicates that they are mainly α-Si_3N_4. It is very difficult to measure the actual linear length of the individual whiskers because of their very curled or coiled forms. The SEM images of the as-synthesized Si_3N_4 microcoils are shown in Figure 1. The majority of the as-synthesized materials are regular coils with the coil pitch and coil diameter constant through the coils (Fig. 1a). Displayed in Figure 1b is a SEM image of a well-formed spring-like whisker, which is very similar to a typical miniature telephone cord. Figure 1c and d demonstrate the high degree of uniformity of the microcoils, in which both right- and left-handed chiralities have been observed with the same probability, indicating the microcoil has no preference either in left-handed or right-handed chirality. The surface of the whiskers is very smooth and no grains or impurities are observed.

To achieve real applications in industry, some important issues about the microcoiled Si_3N_4 whiskers have to be made clear in advance. Can the microcoils recover their original shapes when loaded/unloaded several times and whether the spring constants are variable in the repeating loadings. According to the characteristic of spring: after stretching the spring to ultimate length five times, we suppose there is no permanent distortion for the spring if the length difference between the fourth and the fifth cycle is less than a certain value of its original length.[25] So we choose five cycles as a criterion to prove the spring properties of the microcoiled Si_3N_4 whiskers. A tensile-loading manipulation with the pulling rate of $0.015\ mm\ S^{-1}$ was conducted on one microcoil. The dimensions of the microcoil used in this case were approximately $D = 160$ μm, $L = 2$ mm, $d = 2.4$ μm, and $H = 200$ μm. To avoid the microcoil being broken at the start, it

[*] Prof. C. B. Cao, Dr. H. L. Du, Dr. Y. J. Xu, Prof. H. S. Zhu
Research Center of Materials Science, Beijing Institute of Technology
Beijing 100081 (P.R. China)
E-mail: cbcao@bit.edu.cn
Prof. T. H. Zhang, R. Yang
LNM, Institute of Mechanics, Chinese Academy of Science
Beijing, 100080 (P.R. China)

[**] The work was supported by the Natural Science Foundation of China and the Research Foundation for the Doctoral Program of Higher Education of China.

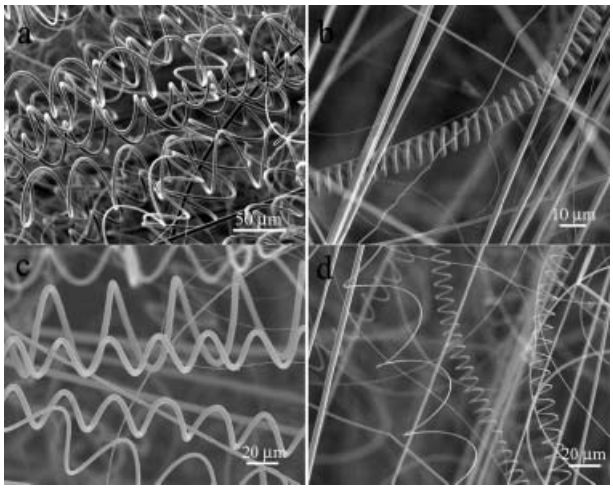

Figure 1. SEM characterization of the as-synthesized silicon nitride microcoils.

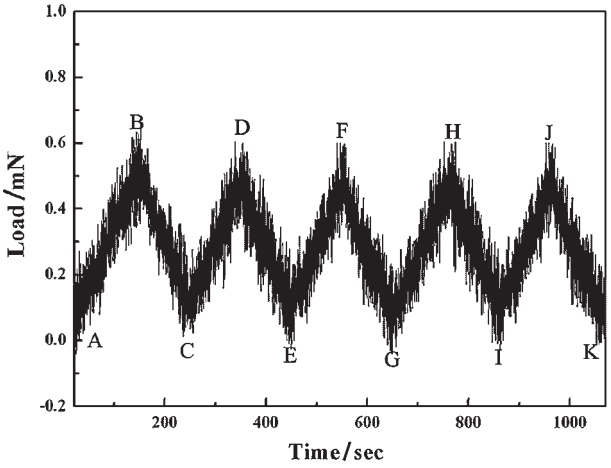

Figure 2. The curves of applied load versus time of the microcoil by extending 1.5 mm in tension, unloaded five times.

was first prestretched to 1.5 mm, then extended it in loaded, unloaded five times at the scale of 0–1.5 mm and examined the process in the screen. The corresponding curve of applied load versus time of the microcoil is shown in Figure 2. From A to B is the first loading process and from the point marked B in Figure 2, the testpiece starts to be unloaded to the original position C before once again the extension, which is the first cycle. Note that the loading and unloading curves are all linear. On the basis of Hook's Law, the spring constant K can be calculate from the load and elongation data, which can be expressed as follow: $K = F/\Delta L = F/vt$, where F is the applied tensile force on the microcoil, ΔL is the total elongation, v and t are the pulling rate, time, respectively. The linear fit value for K_1 of the course AB is $0.32\,\mathrm{Nm}^{-1}$. Moreover, in each loading cycle, the curves of loading and unloading are symmetrical, i.e., the slope of the unloading is opposite to that of the loading process, suggesting that the deformed microcoil eventually restores to its original shape. Similar phenomena are also observed in the rest loading cycles. The linear fit value for K_2 of the course CD, K_3 of the course EF, K_4 of the course GH, K_5 of the course IJ are $0.33\,\mathrm{Nm}^{-1}$, $0.31\,\mathrm{Nm}^{-1}$ $0.30\,\mathrm{Nm}^{-1}$, and $0.32\,\mathrm{Nm}^{-1}$, respectively. Comparing the five spring constants, the values of them are almost equal in the scope of error, indicating the elasticity of the microcoil can keep steady after undergoing several times of stretching.

When the extension distance was prolonged to 2.5 mm (the stretched microcoil had reached to an almost straightened shape in this case.) and the pulling rate was set at $0.03\,\mathrm{mm\,S}^{-1}$, the response of load versus time was different from the previous one. Although the microcoil could return to its initial state, the spring constant K in each loading process would rather increase with increasing relative elongation at high elongation range. Figure 3 recorded the sequential elastic deformation and recovery process of the microcoil for five loading cycles at the scale of 0–2.5 mm. Figure 3a shows the helical whisker relaxed prior to loading with two ends adhesive to the opposite sides of a card. Figure 3b shows the same microcoil after being pulled on the upper end, which causes the microcoil extend along the pulling direction. At first, the helical whisker clearly expands at the front part, while at the same time the lower part of the whisker is not obvious deformation. With the gradually increasing of the loading, extension deformation produces decreasing in coil diameter D and increasing in coil pitch H (Fig. 3b and c). We extend continuously again at the same part and observe that it is further expanded. It is surprising to find that the microcoil can be pulled to an almost straightened shape without broken. The photo in Figure 3d reveals that the

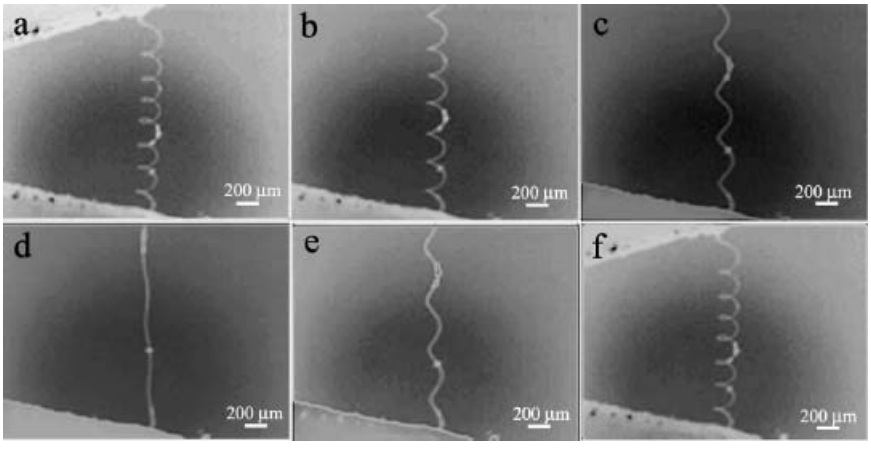

Figure 3. When the extension distance was prolonged to 2.5 mm, a series of photos were taken in the first loaded/unloaded process.

ADVANCED MATERIALS

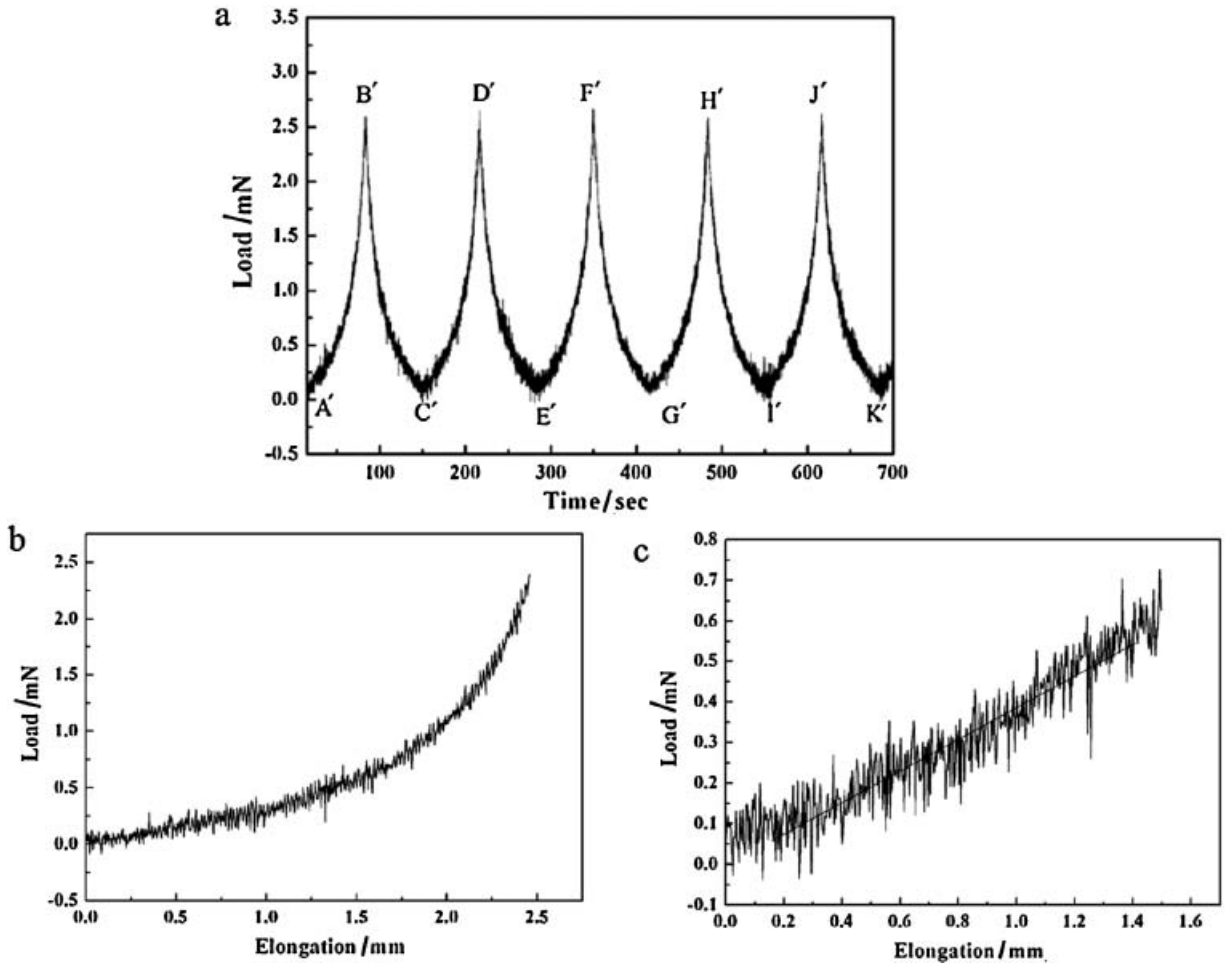

Figure 4. The tensile curves of the microcoil by extending 2.5 mm in tension, unloaded five times. a) The curves of applied load versus time of the microcoil by extending 2.5 mm in tension, unloaded five times. b) Load versus elongation response of the microcoil in the first loading process. c) Load versus elongation response of the microcoil at low-strain region.

extended microcoil has reached an extreme extension and the helical shape is inevident. Instead, only a segment of straight wire is distinct. No separation or sliding at the ends is observed. After reaching the maximum relative elongation, the load is slowly released. In Figure 3e, the stretched microcoil has obviously begun to recover its shape from the extreme extension displayed in Figure 3d. A careful comparison the microcoil dimensions presented in Figure 3a and f indicates that the microcoil has an almost identical dimensionality, suggesting a complete elastic recovery. It can be seen that the helical morphology of the source microcoil is perfectly preserved. Such maneuvers are performed for another four cycles and the same reversible behaviors shown in Figure 3a–f are observed in the process of the latter loading cycles. That is, even stretched to an almost straightened shape several times, the microcoil can also recover its original state after releasing the load and no damage happens to it, which displays the superelasticity behavior of the Si_3N_4 microcoil. This is certainly not possible with traditional steel springs. The superelastic effect has been discovered in nanohelices.[24] However, in the microscale, the superelasticity still occurs for the Si_3N_4 coils and the exact mechanism behind this need further investigations.

The curve of applied load versus time of the microcoil for the case of Figure 3 is shown in Figure 4a. The relationship between the applied load and time is not linear. However, in each loading cycle, the loading and unloading parts are still symmetrical. At the points marked B′, D′, F′, H′, and J′, the testpiece starts to be unloaded and finally gets to its original position C′, E′, G′, I′, and K′, which constitutes the five loading cycles. The slope of the curve is interested here: In each loading cycle, a linear region begins from the start of loading followed by an increasing of the slope (Fig. 4b) and from the low-elongation data of Figure 4b, a linear fit value for K_1' of $0.32\,Nm^{-1}$ is obtained (Fig. 4c). It indicates that the spring constant of the microcoil increases with increasing of relative elongation at high-strain region. At high-strain region, the spring constant can be increased continuously to $3.8\,Nm^{-1}$.

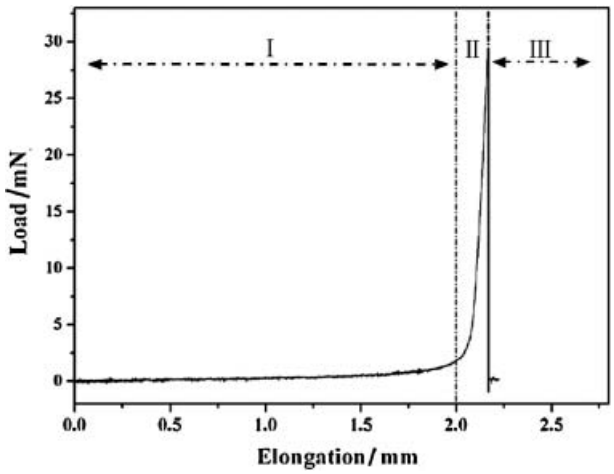

Figure 5. Load-elongation curve of the entire stretching and breaking process of a microcoil. On the basis of observations, it is assumed that stage I corresponds to conversion process of the coil wire into a straight, taut configuration. Stage II and stage III represent the elastic and fracture strain of the microcoil, respectively.

Similar phenomenon have been found in carbon and ZnO nanocoils.[24,26]

When the applied load exceeded the endurance of the microcoil, continually tensile manipulation would lead to the break of the microcoil with fast recoil of the broken segments. But the microcoil does not slip relative to the card, revealing that the attachment between the microcoil and the card is very strong. Figure 5 shows the load versus elongation measured during a microcoil stretching. Similar load-elongation curves were obtained for the other Si_3N_4 microcoils. The load-elongation curve can be divided into three stages.

In stage I, the microcoil straightened by pulling the upper grip is relatively low-energy process that leads to large changes in the coil radius and pitch distance of the Si_3N_4 microcoil. With the gradually increasing of the loading, extension deformation produces decreasing of coil diameter and increasing of coil pitch. Finally, the helical shape is inevident, instead, only a segment of straight wire is distinct. We refer to this step as conversion of the coil wire into a straight, taut configuration and believe this stage is reversible.

Stage II is an elastic domain, where a comparatively larger load is required to extend the taut wire. As elongation increases, the load rises much faster in stage II than in stage I. From the slope of the load-elongation curve in stage II, the Young's modulus of the Si_3N_4 material can be deduced.

Stage III is a fracture domain, in which some segment of the Si_3N_4 microcoil is stretched beyond the elastic limit, then followed a sharp drop in load. After breakage, the broken segments recoil quickly toward their respective ends.

The strains at which failure occurred for the Si_3N_4 microcoils were generally 80–300%. In fact, the obtained values were smaller than their true values because the Si_3N_4 microcoil tested for the tensile experiment was a broken segment of the longer Si_3N_4 microcoil that had been stretched previously in the course of preparing the testpiece. Consequently, the measured strains at which failure occurred for the Si_3N_4 microcoils were slightly less than their true values.

Tensile strength (TS) is a measure of the ability of a material to resist stretching forces. It is obtained by dividing the maximum load a body can bear before breaking (F_{break}) by the cross-sectional area (A) at the break point.

$$TS = \frac{F_{break}}{A} \tag{1}$$

In this study, the cross section (A), assumed circular, is set equal to the cross section of the primary coil whisker which is $\pi d^2/4$ that can be estimated from the SEM image. The breaking forces and cross-sectional areas of each whisker at the point of breaking were determined for different microcoils. These microcoils had dimensions of coil diameter ranging from 50 μm to 250 μm, coil pitch ranging from 120 μm to 400 μm, d ranging from 1.24 μm to 3.2 μm. Then the tensile strength of each

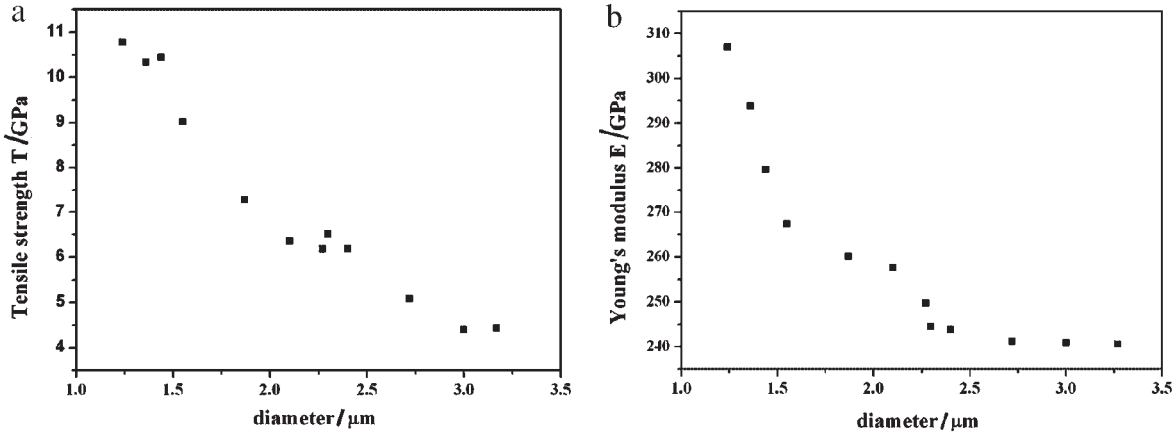

Figure 6. Relationship between the tensile strength *T*, the Young's modulus *E* and the diameter of the coiled whisker. a) The tensile strength is approximately proportional to the diameter of coil whisker *d*. b) Relationship between the Young's modulus *E* and the diameter of coil whisker *d*.

ADVANCED MATERIALS

individual Si_3N_4 microcoil is obtained using Equation 1. The result showed the tensile strength was in the range of 4.5–11 GPa and was closely related to the diameter of the coil whisker. The relationship between the tensile strength T and the diameter of coil whisker d was plotted in Figure 6a. From the curve it can be seen that the tensile strength and the diameter of the coil whisker are approximately linearly related. The smaller the diameter of the coil whisker results in a larger tensile strength. The high value of tensile strength may be due to the low occurrence of defects in the microscale devices.

Young's modulus (E) is also a measure of the resistance of a material to deformation. According to Hook's law, the Young's modulus (E) of material is given by Equation 2.

$$E = \frac{\sigma}{\varepsilon} = \frac{F/A}{\Delta L/L} \tag{2}$$

Where σ is the tensile stress, ε is the strain, F is the applied load, A is the cross-sectional area of the coil whisker, ΔL is the change in length and L is the unwound length of a coil whisker. On the basis of the experimental data acquired from the tensile manipulation, the Young's modulus is deduced from the data of linear part of the region of stage II in the entire stretching and breaking process (Fig. 5). Previous testpieces had also been used for estimate the Young's modulus. The result showed the calculated Young's modulus was in the range of 240–305 GPa and had a noticeable dependence on the diameter of the coil whisker. The relationship between the Young's modulus E and the diameter of coil whisker d was plotted in Figure 6b. The curve shows a trend that with the decreasing of the diameter of coil whisker, Young's modulus gradually increases. However, they are not linearly related. The curve can be divided into two parts. In the part of d is less than 2.25 μm, the Young's modulus increases rapidly with the decreasing of d. While the value of d is bigger than 2.25 μm, the Young's modulus changes slowly with the increasing of d and shows roughly constant. These results show that the Young's modulus of Si_3N_4 microcoil is affected significantly in the small diameter of coil whisker regime. It is anticipated when the diameter of coil whisker is at the scale of the nanometer, the Young's modulus of Si_3N_4 microcoil would be much higher than that of its bulk counterpart. In this study, the assumed constant of cross section area during stretching leaded to a larger cross section area than that at the breaking point, resulting in smaller tensile strength and Young's modulus values.

In summary, a series of monotonic and cyclic loading tests were conducted on Si_3N_4 microcoils manufactured from CVD method. The combined Instron microtester/photo mechanics tool system makes possible quantitatively study of the mechanical behavior of Si_3N_4 microcoil under tensile stress. The microtester allows force measurements in the range of submicronewtons while simultaneously the photo mechanics tool permits visual observation of the structural changes during stretching. The tensile reversibility of the microcoils under cyclic loadings, which has not been described before, may well demonstrate the superelasticity of the Si_3N_4 microcoils and their spring properties. The spring constant of them showed changeless with increasing cyclic loadings, which exhibited the stability of their tensile property. The resulted load-elongation data permitted the calculation of the breaking force, tensile strength and Young's modulus. Based on measurements with different whisker diameter microcoils, we had obtained the relationship between the tensile strength and the diameter of coil whisker. They were approximately linearly related and the tensile strength was in the range of 4.5–11 GPa. The Young's modulus was in the range of 240–307 GPa, which had a noticeable dependence on the diameter of coil whisker. Generally speaking, the tensile properties of the Si_3N_4 microcoils were not degraded significantly under cyclic loadings. The good performance of the microcoils makes them as valuable building blocks in the development of future microscale devices with the advantage of surviving high temperatures or harsh environments and the practice of using the results from cyclic loading tests for microdevice designs, such as elastic energy storage, buffer, indicator and transducer, appears reasonable.

Experimental

Preparation of Microcoiled Si_3N_4 Whiskers: The synthesis of microcoiled Si_3N_4 whiskers was performed in a horizontal tube furnace using pure silicon powder and silica powder as raw materials which were placed into an alumina boat and then loaded into the central region of a ceramic tube. After the tube had been purged with NH_3 for 15 min, the NH_3 flow-rate was set at 70 sccm (standard cubic centimeters per minute) during the entire experiment. The temperature at the central region of the furnace was increased to 1350 °C at the ramp rate of 8 min^{-1} and then maintained at this temperature for 4 h. After the furnace had cooled to room temperature, a quantity of gray white wool-like product was deposited on the top of the source materials. A LEO 1530 field emission scanning electron microscopy was used to characterize the product.

Cyclic Tensile Experiment: Elasticity characteristics of a single microcoiled Si_3N_4 whisker was actually studied by extending it using an Instron 5848 microtester under loading/unloading cycles. For the tensile loading experiment, the sharp tip of the tweezers was brought into contact with one end of a selected microcoil protruding from the bulk sample under an optical microscopy and then a single microcoil testpiece was made by gluing a coil gauge length over a hole in a card, adhesive bonding the ends to the card. This piece was then used as a microcoil source for our tensile measurements. Firming the microcoil attachment onto the card is critical. For the microcoils in the current sample set, a few samples would become detached at one of the ends during the tensile loading experiment. We report here the results from the successful mounting, tensile loading and breaking of the testpieces. Finally, cutting through the edges of the hole before loading and then the loading experiments were conducted in which the coils were monotonically loaded/unloaded in tension by gradually moving the upper grip. When loading, the top grip is driven upward, while the lower grip is fixed, then the microcoil is stretched from its initial length of L to $L + \Delta L$. When unloading, the top grip is driven downward until returning to the original state. A photo mechanics tool attached to the testmachine is used to monitor structural change over time as the microcoil is subjected to repeating loading and unloading cycles. Simultaneously imaging the structural changes in the microcoil during the loading/unloading cycle enables the real-time measurements of the displacement to the applied load. The spring constant is then calculated as the applied load divided by the vertical displacement of the top point in each case. Tensile strength (TS) is obtained by dividing the maximum load a body can bear before breaking (F_{break}) by the

cross-sectional area (A) at the break point. The Young's modulus of the material is determined from the slope of the linear part of the stress-strain curve in a region of elastic behavior.

Received: April 30, 2007
Revised: October 27, 2007
Published online: April 11, 2008

[1] J. A. Roberts, in *Spring Design and Calculations*, Stechert Hafner, New York **1951**.
[2] I. Chen, A. Rosenflanz, *Nature* **1997**, *389*, 701.
[3] F. L. Riley, *J. Am. Ceram. Soc.* **2000**, *83*, 245.
[4] H. Cui, B. R. Stoner, *J. Mater. Res.* **2001**, *16*, 3111.
[5] W. Q. Han, S. S. Fan, Q. Q. Li, B. l. Gu, X. B. Zhang, D. Yu, *Appl. Phys. Lett.* **1997**, *71*, 2271.
[6] J. Q. Hu, Y. Bando, Z. W. Liu, F. F. Xu, T. Sekiguchi, J. H. Zhan, *Chem. Eur. J.* **2004**, *10*, 554.
[7] L. W. Yin, Y. Bando, Y. C. Li, Y. B. Li, *Appl. Phys. Lett.* **2003**, *83*, 3584.
[8] W. Y. Yang, Z. P. Xie, J. J. Li, H. Z. Miao, L. G. Zhang, L. N. An, *J. Am. Ceram. Soc.* **2005**, *88*, 1647.
[9] Y. J. Xu, C. B. Cao, Z. Chen, J. Li, F. C. Wang, H. N. Cai, *J. Phys. Chem. B* **2006**, *110*, 3088.
[10] S. Amelinckx, X. B. Zhang, D. Bernaerts, X. F. Zhang, V. Ivanov, J. B. Nagy, *Science* **1994**, *265*, 635.
[11] S. Iijima, *Nature* **1991**, *354*, 56.
[12] P. X. Gao, Y. Ding, W. J. Mai, W. L. Hughes, C. S. Lao, Z. L. Wang, *Science* **2005**, *309*, 1700.
[13] C. Kuzuya, I. Wan, Y. Hishikawa, S. Motojima, *Chem. Vap. Depos.* **2002**, *8*, 57.
[14] D. N. Mcllroy, D. Zhang, Y. Kranov, *Appl. Phys. Lett.* **2001**, *79*, 1540.
[15] Y. Qu, J. D. Carter, T. Guo, *J. Phys. Chem. B* **2006**, *110*, 8296.
[16] D. Zhang, A. Alkhateeb, H. Han, H. Mahmood, D. N. Mcllroy, *Nano Lett.* **2003**, *3*, 983.
[17] V. Bajpai, L. Dai, T. Ohashi, *J. Am. Chem. Soc.* **2004**, *126*, 5070.
[18] H. F. Zhang, C. M. Wang, E. C. Buck, L. S. Wang, *Nano Lett.* **2003**, *3*, 577.
[19] H. F. Zhang, C. M. Wang, L. S. Wang, *Nano Lett.* **2002**, *2*, 941.
[20] A. Volodin, M. Ahlskog, E. Seynaeve, C. V. Haesendonck, A. Fonseca, J. B. Nagy, *Phys. Rev. Lett.* **2000**, *84*, 3342.
[21] S. Motojima, S. Ueno, T. Hattori, K. Goto, *Appl. Phys. Lett.* **1989**, *54*, 1001.
[22] S. Motojima, T. Yamana, T. Araki, H. Iwanaga, *J. Electrochem. Soc.* **1995**, *142*, 3141.
[23] H. Iwanaga, M. Kawaguchi, S. Motojima, *Jpn. J. Appl. Phys., Part 1* **1993**, *32*, 105.
[24] P. X. Gao, W. Mai, Z. L. Wang, *Nano Lett.* **2006**, *6*, 2536.
[25] A. M. Wahl, *Mechanical Springs*, McGraw-Hill, New York **1981**.
[26] X. Q. Chen, S. L. Zhang, D. A. Dikin, W. Q. Ding, R. S. Ruoff, L. Pan, Y. Nakayama, *Nano Lett.* **2003**, *3*, 1299.

